A study of panel ridges effect on heat transfer and pressure drop in a ventilation duct

Thiago Santos[*1,2], Maria Kolokotroni[1], Nick Hopper[3], Kevin Yearley[3]

[1] *Institute of Energy Futures, Brunel University London, Kingston Lane, Uxbridge, UB8 3PH, UK*

[2] *Federal Institute of Pernambuco, Av. Prof Luiz Freire, 500, Recife/PE –Brazil*
**Corresponding author:*
thiagosantos@ipojuca.ifpe.edu.br

[3] *Monodraught Ltd.*
Halifax house, Halifax Road, High Wycombe, UK

ABSTRACT

CFD simulations were conducted to assess turbulent forced convection heat transfer and pressure drop through a ventilation channel using a stack of panels with different ridge configurations containing Phase Change Material (PCM). First, an experimental rig using an existing commercial panel provided by a PCM manufacturer validates the model simulated in Ansys FLUENT. After that, 3D simulations with different designs were tested until the optimum configuration in terms of heat transfer and pressure drop was achieved. The optimum design by geometry and performance was drawn in 2D and a parametric analysis was performed by varying the spacing between ridges, height and ridge radius to identify difference in heat transfer performance. For both experiment and simulation, the flow rate in terms of Reynolds number based on the inlet hydraulic diameter of the channel ranged from 7200 to 21600. When compared with a flat and existing commercial panel, results show that the inclusion of ridges increase the Nusselt Number by 68 and 93% respectively at a Reynolds number of 21600. At a Reynolds number of 18736, the Nusselt number of the optimum panel is enhanced by 64 and 111% when compared to the flat and existing commercial panel, respectively. This panel was then taken forward to allow further refinements which include changes in panel thickness and number of panels per module. After more than 200 different panel designs and airflows simulations, a new design is proposed which reduces the number of panels per module from 9 to 6, thus reducing production costs but keeping nearly the same heat flux and pressure drop as the existing commercial panel. When 7 panels are used, it is possible to hold 13.68% more material with an increased pressure drop 3.36 times higher than the existing commercial panel (176.80 against 52.69 Pa) at a Reynolds number of 18736.

KEYWORDS: PCM-Air heat exchanger, Numerical simulation, Rib shape, Heat transfer enhancement/augmentation, Ventilative Cooling

1 INTRODUCTION

PCM-air heat exchangers are one of many thermal storage systems (TES) application in constant study and development (Alizadeh & Sadrameli, 2016). The equipment use the principle of thermal storage through latent heat in climates where night temperatures are cold enough to charge (solidify) the PCM and use it to cool the environment during the day. The concept has been studied extensively (Arzamendia Lopez *et al.*, 2013; Zalba *et al.*, 2004; Dolado *et al.*, 2011; Lazaro *et al.*, 2009) and performance in practice evaluated (Santos, Hopper & Kolokotroni, 2016; Kolokotroni, Santos & Hopper, 2016). The Phase Change Material in heat exchangers is commonly encapsulated in envelopes with small heat transfer efficiency. Thus, the increase of heat transfer between air and panel will increase the overall performance of the exchanger and lead to a fast thermal response, fast charging period and reduce energy consumption.

The introduction of ridges, fins, dimples and grooves are techniques commonly used to increase the heat transfer over a channel. These turbulators are widely applied and studied in engine turbine blades to protect them from exceeding the maximum allowable temperature.

In PCM-air heat exchangers, turbulators are used to increase cooling performance. However, turbulence also enhances pressure drop and consequently, an oversized fan is needed which will increase energy demand. Alternatively, a design with higher thermal efficiency and small pressure drop is desired and a motivation for researchers.

Nomenclature

Symbols

ΔT	temperature difference (K)	$C_{p(air)}$	Specific heat of air (J/kg·K)
T	temperature (°C)	Nu	Nusselt number
e	Ridge height (m)	Nu_o	Nusselt number over a smooth surface
h	Channel gap (m)	h	Heat convection coefficient (W/m^2)
s	Ridge spacing (m)	D_h	Hydraulic diameter (m)
l	total surface length (m)	k	Thermal conductivity (W/m^{2}K)
r	Ridge radius (m)	A	Area (m^2)
E	Sum of gaps (m)	L	Length (m)
H	Total height (m)	W	Width (m)
p	Pitch (m)	Δp	Pressure difference (Pa)
T_t	Sum of panel thickness (m)	Δp_o	Pressure difference of a smooth surface (Pa)
$\dot{m}$	Mass flow (kg/s)	Q̇	Heat Flux (W)
Re	Reynolds number	η	Efficiency

Subscripts

air	
i	Inlet
o	Outlet
m	Fluid
s	Surface

Abbreviations

LMDT	Logarithmic Mean Difference Temperature
PCM	Phase Change Material
TES	Thermal Storage System
CFD	Computational Fluid Dynamics

Moon (Moon, Park & Kim, 2014) analysed sixteen ridge shapes (with different geometries) by varying pitch ratio. Results show that boot shaped ridge present the best results in terms of heat transfer with a pressure drop similar to a square ridge for a Reynolds number between 5000 and 50,000. The inclusion of dimples, protrusions or both dimples and protrusions also shows good results in heat transfer augmentation. Liu et al (Liu *et al.*, 2015) found that secondary protrusions cause downward flow, reducing recirculation in the adjacent primary dimple and improving the reattachment. In all cases studied, the area-averaged ratio between Nusselt and Nusselt over a smooth surface (Nu/Nu_o) enhanced in 1.8 and 1.5 times for Reynolds ranging from 5000 to 27,500. Yang et al. (Yang *et al.*, 2017) introduced symmetric and staggered squared high ridges in channels with results showing that a larger blockage ratio corresponds to a larger heat transfer coefficient and also a higher friction factor with symmetric arrangement and higher blockage increasing Nu/Nu_o in the range of 6-7 and 3.5 for a staggered arrangement and higher blockage

Promvonge and Thianpong (Promvonge & Thianpong, 2008) experimented with four different shaped ridges (wedge pointing upstream, wedge pointing downstream, triangular and rectangular ridge) staggered and in-line over a turbulent channel ($Re = 4000 - 16{,}000$). The result shows improvements in heat transfer when compared to a smooth channel where the wedge downstream in-line with the best performance in terms of Nusselt number ratio ($Nu/Nu_o \cong 4.4$) and the rectangular ($Nu/Nu_o \cong 3.7$), the worst. When pressure drop is taken into account, the triangular staggered has the best thermal performance $\left(\eta = \left(\frac{Nu}{Nu_o}\right)/\left(\frac{\Delta p}{\Delta p_o}\right)^{1/3} \cong 1 - 1.1\right)$ followed by triangular in line and staggered upstream wedge. After that, Thianpong et al. (Thianpong *et al.*, 2009) experimentally studied different heights of triangular ridges staggered and in-line through a constant heat-fluxed channel for Reynolds number of 5,000 to 22,000. The result shows an increase of approximately 1.8 – 4 in terms of

Nusselt number when compared to a smooth channel and a variation of thermal performance up to 1.3.
The present study focusses on the design of a panel surface able to enhance the heat transfer efficiency of PCM-air heat exchangers where pressure loss is an important parameter for systems requiring low power demand and noise levels.

2 METHODOLOGY

The designing process of the panel started by using existing literature as a basis where rounded ridges were selected for the PCM panel due to the reduced pressure drop, relative ease in manufacture and lower cost of production.

Figure 1: Existing panel in use for the PCM-Air heat exchanger (Rubitherm)

First, ten 3D designs were evaluated in terms of heat transfer and pressure drop through CFD simulations over a section of one panel channel and compared with the existing panel (Figure 1) in use and a dimpled panel. Each design was drawn with different rounded losange, protrusion and groove radius and also height and pitch. Surface temperature is fixed at 20 ^{o}C because is a melting point of a PCM used for this application and an inlet channel temperature of 26 ^{o}C is a common return air through recirculation or an outside air during cooling periods. The mesh was generated as coarse and adapted through Ansys FLUENT until no changes on the fourth decimal case of inlet pressure and outlet temperature were found, the turbulation model used was realizable $R-\varepsilon$ with scalable near wall treatment function and under-relaxation factors were adjusted to allow convergence and simulation stops when residuals achieved 10^{-5}. The flow rate in terms of Reynolds number were based on the inlet hydraulic diameter of the channel and ranged from 7,200 to 21,600. The results were compared and one design uniform along its width was selected due to easy in manufacture for a more detailed analysis. Moreover, an experiment using the existing panel with 1, 2 and 3 modules measured and analysed the pressure drop through the channel and validated the CFD model. Results show that even if the existing panel is not uniform along its width, simulations in 2D present sensible results compared to the experiment measurements with a maximum difference of 16.05 Pa (or -23.85%) for 3 modules at *Re* = 21,600 and 0.77 Pa (or -6.96%) for *Re* = 10,089 and 2 modules. This higher pressure drop compared to the experimental values was expected because the PCM panel has an undulated surface on the existing panel and simulations considered the plane on top of the undulation. To validate the heat transfer simulation, temperature data of one unit installed in a seminar room was used. The temperature before and after the PCM was stable for a couple of hours and the average of that was assumed to be the panel surface temperature.
Furthermore and based on the optimum design by geometry and performance of the first set of simulations, 13 surface geometries were generated in 2D to perform a parametric analysis varying ridge height (ridge height/channel gap) $[0.0625 < e/h < 0.3125]$, ridge pitch (ridge spacing / total surface length) $[0.0223 < s/l < 0.0558]$ and ridge radius $[2.5 < r < 7.5]$

evaluate pressure drop and heat transfer efficiency. These dimensions are represented in Figure 2.
The optimum design was again selected for further refinements by generating 9 surfaces to evaluate the gap between panels (sum of gaps/total height) $[0.254 < E/H < 0.397]$, panel thickness (sum of panel thickness/total height) $[0.6032 < T_t/H < 0.7460]$ and number of panels $[4 < p < 9]$ with the final design being used to fabricate the panel.

2.1 Heat transfer:

The heat transfer between panels and air was calculated by the energy balance through the air crossing the volume control and is given by:

$$\dot{Q}_{air} = \dot{m}_{air} C_{p(air)} (T_o - T_i) \quad \text{(W)} \qquad (2.1)$$

Where: $\dot{m}_{air}$ is the air mass flow rate in $\frac{kg}{s}$; $C_{p(air)} = 1006.43\ [\frac{J}{KgK}]$; $T_i = 26^o C$; T_o is the air outlet temperature calculated by CFD, $\dot{Q}_{air}$ is in Watts and is assumed that there are no losses through the walls.

2.1.1 Nusselt number and convective heat transfer coefficient:

Nusselt number is a dimensionless term equal to the temperature gradient on the surface and provides the ratio between convective and conductive heat transfer (Incropera, 2007) given by:

$$Nu = \frac{hD_h}{k_{air}} \qquad (2.2)$$

Where D_h is the hydraulic diameter, k_{air} is the thermal air conductivity and h is the convective heat transfer coefficent.
To evaluate h, a control volume is applied (Figure 2) and all energy released by the air $(\dot{Q}_{air})$ is absorbed through convection $(\dot{Q}_c)$ by the panel (Eq. (2.3).

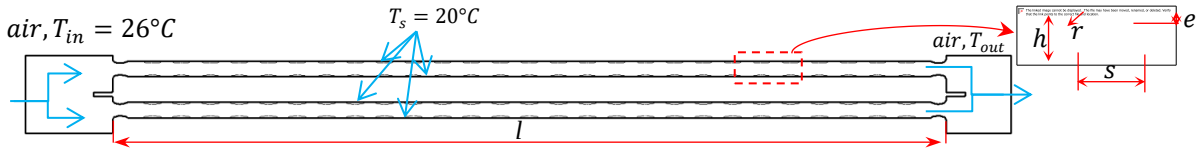

Figure 2: PCM panel control volume

$$\begin{gathered} \dot{Q}_{air} = \dot{Q}_c \\ \dot{m}_{air} C_{p(air)} (T_{out} - T_{in}) = h A_{panel} \Delta T \end{gathered} \qquad (2.3)$$

Where $A_{panel} = L_{panel} \cdot W_{panel}$. For cases using constant surface temperature, the difference between hot and cold is given by a logarithmic mean temperature difference ΔT_{LMDT} (Incropera, 2007):

$$\Delta T_{LMDT} = \frac{(\Delta T_o - \Delta T_i)}{\ln\left(\frac{\Delta T_o}{\Delta T_i}\right)} = \frac{(T_s - T_{m,o}) - (T_s - T_{m,i})}{ln\left[(T_s - T_{m,o})/(T_s - T_{m,i})\right]} \qquad (2.4)$$

Where $T_{m,o}$ is the outlet fluid temperature; $T_{m,i}$ is the inlet fluid temperature and T_s is the surface temperature. Adding Eq. (2.4) in Eq. (2.3):

$$h = \frac{\dot{m}_{air} C_{p(air)} (T_o - T_i)}{(L_{panel} \cdot W_{panel}) \left(\frac{(T_s - T_{m,o}) - (T_s - T_{m,i})}{\ln\left[\frac{T_s - T_{m,o}}{T_s - T_{m,i}}\right]} \right)} \qquad \left[\frac{W}{m^2 K}\right] \qquad (2.5)$$

2.1.2 Efficiency

The introduction of ridges requires more pumping power from the system. The thermal enhancement factor (Tyagi *et al.*, 2015), η, analyse the ratio of the convective heat transfer of the augment surface over a smooth surface at a constant pumping and is given by:

$$\eta = \frac{\left(\frac{Nu}{Nu_o}\right)}{\left(\frac{\Delta p}{\Delta p_o}\right)^{1/3}} \tag{2.6}$$

Where Nu_o and Δp_o are the Nusselt number and the pressure drop in a smooth panel. Values higher than 1 suggest an increase in heat transfer or reduction on pressure drop when compared to a smooth panel and values lower than 1 suggest the opposite.

3 SIMULATION RESULTS AND DISCUSSION

3.1 3D simulations

The first set of simulations started by generating a batch of ten 3D panels with different configurations at *Re* = 18736 plus the existing panel and dimpled panel as the two examples presented in Figure 3. The control volume is the channel where the air crosses and exchange heat with the panel with Figure 4 showing an example of the section modelled for simulation in Ansys FLUENT.

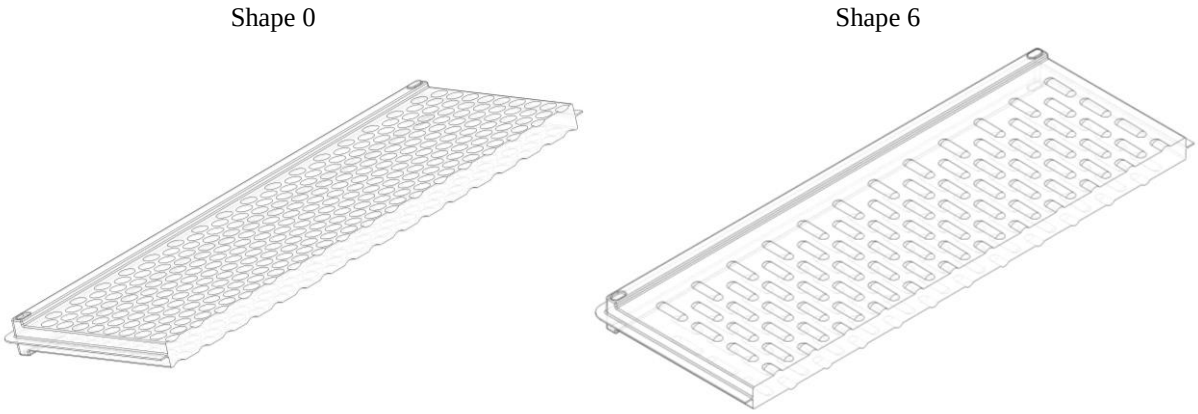

Figure 3: Examples of 2 designs used for 3D simulation.

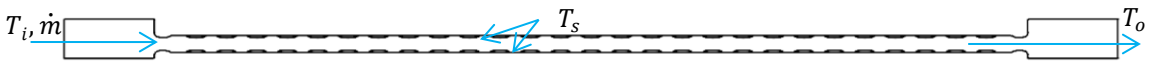

Figure 4: Existing panel sectioned and the section used for 3D simulation.

The results of pressure drop, outlet temperature and heat flux from the 3D simulation are presented on Table 1 sorted by heat flux; shapes 6 and 3 revealed a high heat flux at a cost of a high pressure drop. Alternatively, shapes 2, 1 and 9 show promises in terms of heat transfer in comparison to other shapes with approximately double heat transfer compared to the existing panel with a reasonable increase in pressure drop. Based on these results and due to the simplicity of its design in manufacture, shape 9 was chosen for additional refinements.

Table 1: Pressure drop, outlet temperature and Heat Flux of one 3D panel sectioned at *Re* = 18736

Shape	Pressure drop (Pa)	Outlet temperature (°C)	Heat Flux (W)
6	105.54	21.28	-757.29
3	93.12	21.59	-706.33

2	60.62	21.71	-687.09
1	44.23	21.78	-676.52
9	55.58	21.88	-660.97
8	17.00	22.00	-641.10
0	30.82	22.52	-558.39
5	24.47	22.69	-531.15
10	50.37	23.21	-447.00
4	31.13	23.84	-346.19
Existing	10.58	23.91	-335.61
7	40.49	24.03	-316.54

3.2 2D simulations

In first instance, 13 variations (Shapes 11 to 23) based on Shape 9 were drawn and sectioned along their length for 2D simulation. In each case, 7 panels per module were used to perform a parametric analysis of the spacing between ridges, ridge height and radius. The most effective in terms of heat transfer and pressure drop (Shape 11, Figure 5) was used to generate 9 more cases (Shapes 24 to 32) by varying panel thickness, spacing between panels and total of panels per module.

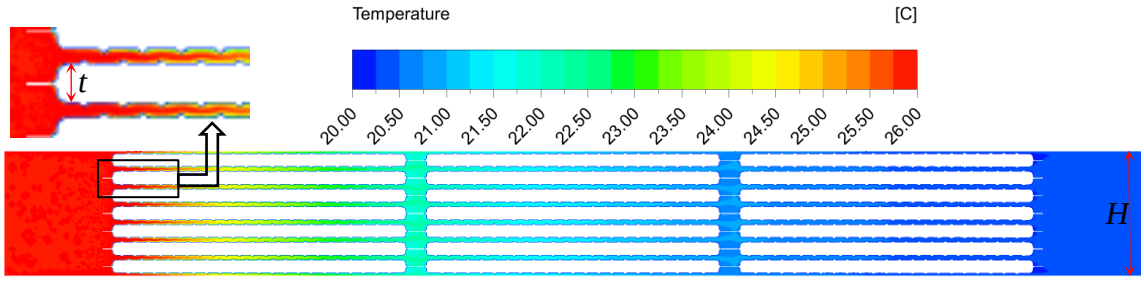

Figure 5: Temperature distribution of Shape 11 at *Re* = 18736

The results presented in Table 3 show that Shapes 11, 24 and 25 have higher Heat Flux compared to the existing panel, with Shape 11 able to transfer approximately 14% more energy at *Re* = 18736 and hold 13.68% more PCM. These shapes have a pressure drop higher than the existing panel. However, fan Head curve (Figure 6) shows that the AHU can provide sufficient pressure at the required airflow to overcome this drop. Furthermore due to the increased energy transfer, less airflow is required over the panels and consequently less electric energy demanded.

Table 3 also shows that Shape 27 displays similar levels of performance to the existing panel in terms of heat transfer and pressure drop. Therefore this arrangement could be integrated with little change to the systems operation. This design would also be seen to reduce costs as only six panels are required per module and the quantity of PCM would be reduced by 2.56% as can be seen on Table 2. This table also shows that shapes 27, 28, 29 and 30 reduce PCM volume even if different amount of panels per module are used due to the increase in panel thickness. Shape 26 has the highest increase in volume and but the higher pressure drop (323.34 Pa at *Re* = 18,736) which makes shape 11 the most reasonable in terms of increase in volume change, pressure drop and heat transfer.

Table 2: Volume change in comparison with existing panel

	11	**24**	**25**	**26**	**27**	**28**	**29**	**30**	**31**	**32**
	13.68%	0.08%	2.63%	20.51%	-2.56%	-2.56%	-2.56%	-2.56%	3.93%	2.31%
Panels per module	7	9	8	6	6	6	5	4	8	9

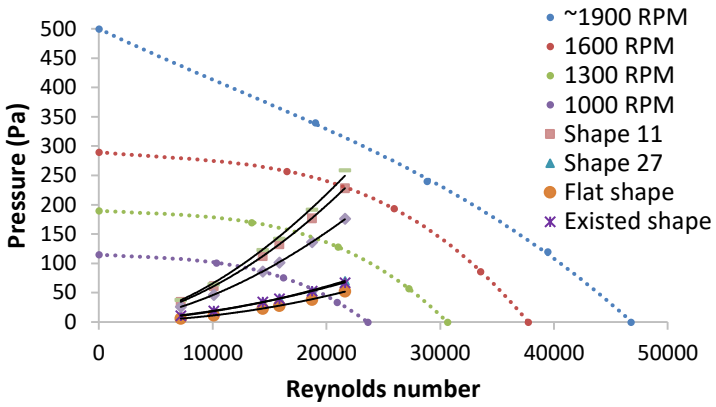

Figure 6: Head curve of panels 11, 24, 25, 27 as well as the Flat and the existing shape with fan curves at different rotation speeds.

The Nusselt number indicates how much energy is exchanged by convection or conduction. When $Nu = 1$, it means the heat transfer is purely by conduction and a higher Nusselt number shows more efficient heat transfer. This makes Shape 29 and the existing panel having the worst performance when compared to other shapes. On the other hand, shape 26, 11 and 24 (Figure 7, right) have the best performance at any Reynolds number evaluated by showing an average increase of 2.2 times for shape 26, 2.02 for shape 11 and 2.03 for shape 24 for Reynolds between 7,200 and 22,000. This increase allows a fast response by the PCM-Air heat exchanger when the heat load increases suddenly. Furthermore, when no air is crossing the thermal batteries, shapes 26 and 11 lose less energy through free convection due to a lower surface area when compared to the existing panel.

When Nusselt number is compared with a smooth surface (Nu/Nu_o), shapes 24, 26 and 11 present the best results, showing an average increase of 2, 1.8 and 1.75. As it can be seen in Figure 7 (left) where the ratio for all cases are presented, the inclusion of ridges favoured heat transfer by the increase of turbulence at lower Reynolds number allowing a reduction in PCM-Air heat exchanger air flow, saving energy and reducing noise. The result also shows that the existing panel perform better than a smooth surface only at low Reynolds numbers (1.27 and 1.09 for 7,200 and 10,089 respectively). For Reynold numbers above 10,089 the existing panel have a performance similar to a smooth panel.

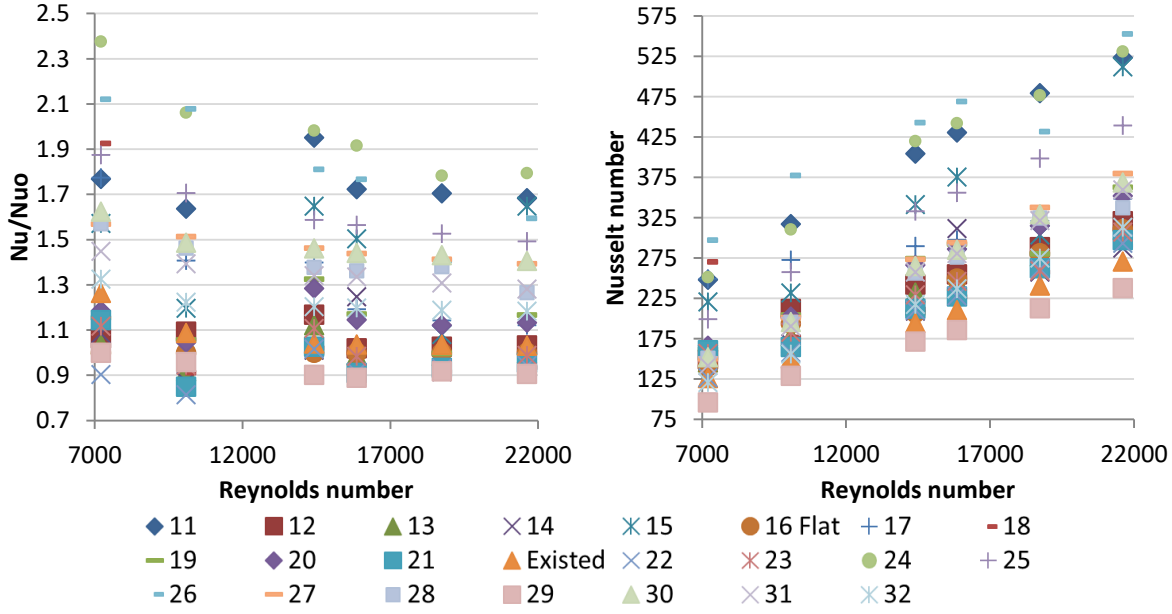

Figure 7: Ratio between Nusselt number and a smooth panel and Nusselt number

Comparing the ratio between Nusselt and pressure drop shows how efficient the panel performs. Figure 8 shows that shapes 11, 24, 25, 27, 28 and 30 have values above 1, which means that the inclusion of ridges enhance the heat transfer at a lower cost in terms of pressure drop when compared to a smooth surface. Values below 1 means that the pressure drop increases in a proportion higher than Nusselt number, leading to an increase of noise and energy cost with a small benefit on heat transfer. Shape 26 has the best performance in terms of Nusselt number but the higher pressure drop lowers its efficiency (0.86 in average).

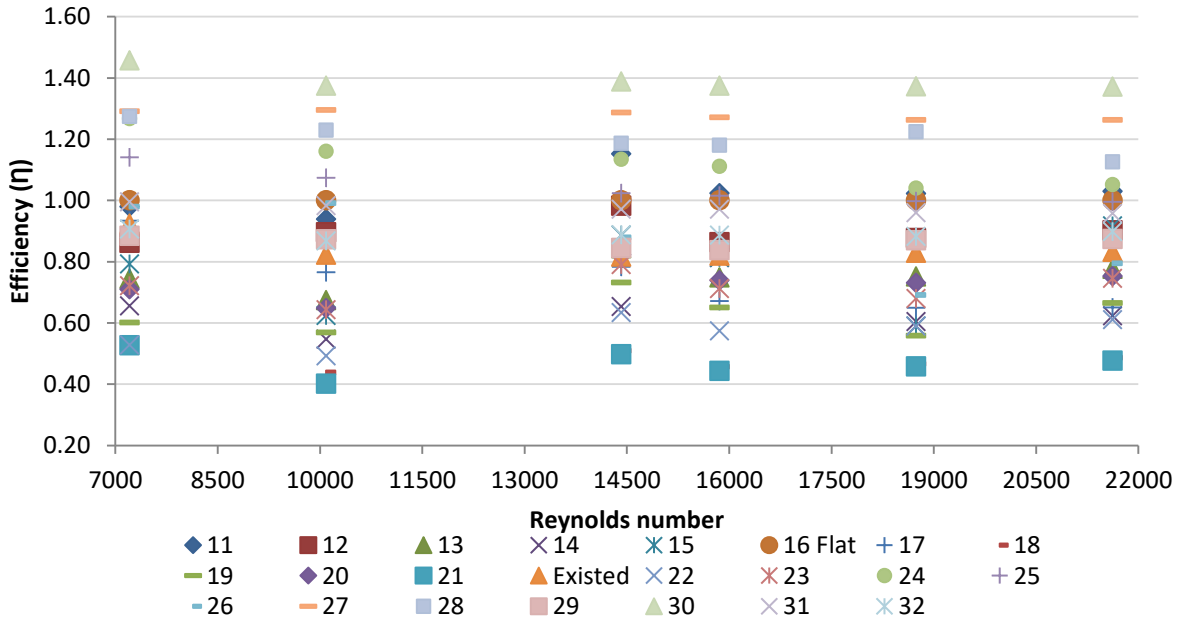

Figure 8: Efficiency

4 CONCLUSIONS

More than 200 simulations were performed with different surface designs and air flows until the optimum design in terms of heat transfer, pressure drop and low production cost was achieved. Shape 11 doubled the heat transfer and holds 13.68% more material than the existing commercial panel. The pressure drop increased by 3 but the fan is capable to provide the required air flow. More power from the fan is demanded but due to the increase of heat transfer a lower air flow will be requested by the PCM-air heat exchanger unit. At present, the developed design is being fabricated and future experimental tests will validate its performance.

5 ACKNOWLEDGEMENTS

The first author would like to thank Science Without Borders program of Cnpq - Brazil, for doctoral funding (PDE: 200815/2014-8).

Table 3: Outlet temperature, Pressure drop and Heat transfer (W) for each shape at *Re* = 10,089 and 18,736.

		Outlet Temperature (°C)		Pressure drop (Pa)		Pressure drop in comparison with existed plate (%)		Heat Flux (W)		Heat Flux in comparison with existing panel (%)		Number of panels per module
	Reynolds	**10089**	**18736**	**10089**	**18736**	**10089**	**18736**	**10089**	**18736**	**10089**	**18736**	
	Existing	293.89	294.14	19.17	52.69	-	-	-453.77	-802.97	-	-	9
	11	293.29	293.44	61.28	176.80	320	336	-505.47	-915.65	11.39	14.03	7
	27	293.95	294.14	18.45	53.43	96	101	-449.03	-802.33	-1.04	-0.08	6
	24	293.43	293.28	46.94	191.98	245	364	-493.64	-941.45	8.79	17.25	9
	25	293.34	293.49	46.35	136.48	375	393	-501.24	-907.63	9.60	4.33	8
	17	293.39	293.92	71.87	207.32	252	261	-497.35	-837.75	3.27	3.13	7
	20	293.72	293.98	48.36	137.64	423	445	-468.62	-828.14	7.00	2.85	7
	15	293.52	294.00	81.14	234.30	556	614	-485.53	-825.89	11.60	2.85	7
	26	293.28	294.00	106.59	323.34	386	412	-506.42	-825.89	3.92	-0.38	6
	19	293.69	294.16	73.99	217.10	152	163	-471.55	-799.93	-0.32	-1.34	7
	28	293.98	294.17	19.46	54.72	86	181	-446.35	-798.81	2.38	-1.34	6
Shapes	**31**	293.66	294.19	32.91	84.17	110	116	-473.54	-795.44	3.27	-1.58	8
	13	293.91	294.21	29.1	86.13	272	284	-452.31	-792.23	-2.78	-2.04	7
	23	293.77	294.21	16.50	95.27	570	612	-464.56	-792.23	-1.56	-2.08	7
	12	293.72	294.22	21.02	60.91	544	550	-468.62	-790.31	1.01	-2.14	7
	22	294.04	294.24	52.22	149.41	60	72	-441.17	-786.62	0.65	-2.79	7
	21	293.97	294.24	109.37	322.44	245	252	-446.70	-786.30	-1.96	-4.21	7
	18	293.84	294.25	104.34	289.60	80	85	-458.35	-785.82	-8.65	-9.62	7
	16	293.86	294.28	11.55	38.09	76	82	-456.71	-780.53	-19.42	-17.92	7
	14	293.99	294.35	46.96	132.91	169	50	-444.88	-769.15	2.72	-24.33	7
	29	294.35	294.62	15.33	44.70	245	364	-414.51	-725.72	8.79	17.25	5
	30	294.91	295.04	14.62	43.21	100	100	-365.66	-659.05	0.00	0.00	4
	32	293.75	295.360	32.41	26.42	320	336	-466.11	-607.60	11.39	14.03	9

6 REFERENCES

Alizadeh, M. & Sadrameli, S.M. (2016) Development of free cooling based ventilation technology for buildings : Thermal energy storage (TES) unit , performance enhancement techniques and design considerations – A review. *Renewable and Sustainable Energy Reviews*. [Online] 58, 619–645. Available from: doi:10.1016/j.rser.2015.12.168.

Arzamendia Lopez, J.P., Kuznik, F., Baillis, D. & Virgone, J. (2013) Numerical modeling and experimental validation of a PCM to air heat exchanger. *Energy and Buildings*. [Online] 64, 415–422. Available from: doi:10.1016/j.enbuild.2013.04.017.

Dolado, P., Lazaro, A., Marin, J.M. & Zalba, B. (2011) Characterization of melting and solidification in a real-scale PCM-air heat exchanger: Experimental results and empirical model. *Renewable Energy*. [Online] 36 (11), 2906–2917. Available from: doi:10.1016/j.renene.2011.04.008.

Incropera, F.P. (2007) *Fundamentals of heat and mass transfer.* John Wiley.

Kolokotroni, M., Santos, T. & Hopper, N. (2016) Ventilative cooling of a seminar room using active PCM thermal storage. *REHVA*. 53 (1), 36–40.

Lazaro, A., Dolado, P., Marín, J.M. & Zalba, B. (2009) PCM–air heat exchangers for free-cooling applications in buildings: Experimental results of two real-scale prototypes. *Energy Conversion and Management*. [Online] 50 (3), 439–443. Available from: doi:10.1016/j.enconman.2008.11.002.

Liu, J., Song, Y., Xie, G. & Sunden, B. (2015) Numerical modeling flow and heat transfer in dimpled cooling channels with secondary hemispherical protrusions. *Energy*. [Online] 79 (C), 1–19. Available from: doi:10.1016/j.energy.2014.05.075.

Moon, M.A., Park, M.J. & Kim, K.Y. (2014) Evaluation of heat transfer performances of various rib shapes. *International Journal of Heat and Mass Transfer*. [Online] 71, 275–284. Available from: doi:10.1016/j.ijheatmasstransfer.2013.12.026.

Promvonge, P. & Thianpong, C. (2008) Thermal performance assessment of turbulent channel flows over different shaped ribs. *International Communications in Heat and Mass Transfer*. [Online] 35 (10), 1327–1334. Available from: doi:10.1016/j.icheatmasstransfer.2008.07.016.

Rubitherm (n.d.) *Rubitherm*. [Online]. Available from: https://www.rubitherm.eu/en/index.php/productcategory/makroverkaspelung-csm [Accessed: 2 May 2017].

Santos, T., Hopper, N. & Kolokotroni, M. (2016) Performance in practice of a ventilation system with thermal storage in a computer seminar room. In: Per Kvols Heiselberg (ed.). *12th CLIMA REHVA World Congress*. 2016 Aalborg. p. 11.

Thianpong, C., Chompookham, T., Skullong, S. & Promvonge, P. (2009) Thermal characterization of turbulent flow in a channel with isosceles triangular ribs. *International Communications in Heat and Mass Transfer*. [Online] 36 (7), 712–717. Available from: doi:10.1016/j.icheatmasstransfer.2009.03.027.

Tyagi, K., Singh, P., Pandit, J., Ramesh, S., et al. (2015) Experimental study of heat transfer augmentation in high aspect-ratio channels featuring different dimple configurations. In: *ASME Turbo Expo 2015: Turbine Technical Conference and Exposition*. 2015 ASME. pp. 1–11.

Yang, W., Xue, S., He, Y. & Li, W. (2017) Experimental study on the heat transfer characteristics of high blockage ribs channel. *Experimental Thermal and Fluid Science*. [Online] 83, 248–259. Available from: doi:10.1016/j.expthermflusci.2017.01.016.

Zalba, B., Marín, J.M., Cabeza, L.F. & Mehling, H. (2004) Free-cooling of buildings with phase change materials. *International Journal of Refrigeration*. [Online] 27 (8), 839–849. Available from: doi:10.1016/j.ijrefrig.2004.03.015.